Research paper

Initial decomposition pathways of guanidium nitrate studied by quantum chemistry calculation

Yu-ichiro Izato*,**† and Atsumi Miyake**

*Graduate School of Environment and Information Sciences, Yokohama National University, 79−7 Tokiwadai, Hodogaya-ku, Yokohama-shi, 240−8501 JAPAN
Phone: +81−45−339−3981
†Corresponding author : izato-yuichiro-hk@ynu.jp

**Institute of advanced sciences, Yokohama National University, 79−5 Tokiwadai, Hodogaya-ku, Yokohama-shi, 240−8501 JAPAN

Received: October 18, 2017 Accepted: April 5, 2018

Abstract

The decomposition mechanism of guanidium nitrate (GN) was investigated by quantum chemistry calculations. Optimized structures of reactants, products, and transition states were obtained at the ωB97X-D/6-311++G(d,p)/SCRF = (solvent = water) level of theory and the total electron energies and free energies of these structures were calculated at the CBS-QB3 level of theory. In the initial decomposition pathway of GN, two mechanisms occur in parallel: CN_3H_5 decomposition and the interaction between CN_3H_5 and HNO_3. The former mechanism has three pathways and each of these schemes provided the same global reaction: $CN_3H_5 \rightarrow HNCNH + NH_3$. Pathways for neutral monomolecular decomposition, neutral-neutral bimolecular decomposition ($CN_3H_5 + CN_3H_5$), and cation-neutral bimolecular reaction ($CN_3H_6^+ + CN_3H_5$) were developed. The latter reaction has four pathways and each of these schemes provided the same global reaction: $CN_3H_5 + HNO_3 \rightarrow HNCNH + N_2O + 2H_2O$. These schemes can be divided according to the combination of oxidizers (HNO_3 or N_2O_5) and reductants (CN_3H_5 or $CN_3H_6^+$). Based on the energy-barrier results, HNO_3-catalyzed monomolecular decomposition in CN_3H_5 decomposition and N_2O_5/CN_3H_5 schemes in the interaction between CN_3H_5 and HNO_3 are the most plausible mechanisms.

Keywords: guanidine nitrate, gas-generation agent, decomposition, liquid-phase reaction, ***ab initio*** calculation

1. Introduction

Energetic compositions rapidly release large amounts of gaseous products, along with exothermic heat; they have been widely used as propellants, fireworks, blasting agents, and gas generants. Gas generants in car-airbag systems must product a large amount of clean gas, which has low toxicity and is environmentally friendly. Clean released gas can prevent a driver and fellow passengers from acute poisoning when a car airbag expands with the evolved gas. In a car airbag, the amount of heat generated from the combustion must also be small because a low-temperature condition allows a plastic sheet to be used as the bag material. In general, plastic sheets cannot withstand high temperatures, but they are extremely effective for reducing the car weight, providing good mileage. The auto industry strongly demands the use of plastic materials for car airbags. Thus, the development and improvement of green propellants that evolve clean released gas and have a small heat of combustion are required.

Guanidium nitrate (GN) is an excellent fuel for a gas-generator propellant because it has high energy content (its enthalpy of combustion is −386.7 kJ mol^{-1})[1], and contains a number of nitrogen atoms. For example, mixtures of GN as the fuel and basic copper nitrate (BCN) as an oxidizer are currently well-established as gas-generating agents; they have been widely applied to car-airbag systems. To improve the combustion properties of GN-based gas generants, many researchers have experimentally studied the decomposition and combustion mechanism[2)−6)] and the effect of various additives on decomposition[4)−10)].

A fuller understanding of the combustion mechanism is required to develop cleaner evolved gas and enable lower combustion temperatures. To this end, combustion simulations based on a detailed chemical kinetic model are effective. Such simulations, which include detailed kinetic information, can provide deep insight into the chemical reactions in a flame and suggest which reactions are key to decreasing the production of harmful gases and the flame temperature. Our previous study provides the kinetic model for gas-phase combustion of GN[11]. However, to the best of our knowledge, there are no detailed reaction models for liquid-phase GN decomposition. The combustion of energetic salts, including GN, is typically characterized by a diverse range of physical and chemical processes that occur in a complex series of stages. In the case of energetic onium salts, the condensed-phase reactions have the greatest effect on the combustion characteristics[12)–14)]. To date, some reliable energetic-salt gas-phase reaction models have been proposed, which explain the observed combustion behavior[14)–22)]. More recently, models for the liquid-phase reactions of these compounds have also been developed[23)–27)]. However, there are no detailed reaction models for the condensed-phase reactions of GN.

To develop a detailed reaction model for the condensed-phase reactions of GN, it is important to understand the thermal-decomposition pathways and associated kinetics. The aim of the present study was to elucidate the reaction pathways involved in liquid GN thermal decomposition based on *ab initio* thermochemistry calculations. The decomposition reaction of GN appears to be a multistep, competitive process. Therefore, we require a detailed understanding of each reaction to establish a clear reaction mechanism. *Ab initio* quantum chemical calculations are helpful in determining which reactions to exclude from the mechanism based on thermodynamic arguments.

2. Computational methods

The geometries of the reactants, products, and transition states (TSs) were optimized at the ωB97X-D/6-311++G(d,p)[28)] level of theory using the Gaussian 09 program package[29)]. Chai and Head-Gordon[28)] developed the ωB97X-D method, which includes empirical dispersion forces and is believed to be reliable when applied to systems with weak van der Waals forces. Their group has also reported that the ωB97X-D method yields satisfactory accuracy for kinetics and non-covalent interactions. During computations, TSs were extensively searched for and, if found, an intrinsic reaction coordinate (IRC) calculation was conducted to assign reactants and products to the TS. The energies of the corresponding molecules were evaluated at the CBS-QB3[30)] level of theory, as this is a reasonable time-expense complete basis method. In this study, geometries and frequencies were calculated at the ωB97X-D/6-311++G(d,p) level of theory, the optimized geometries were fixed with no changes allowed, and the potential energies were calculated using the CBS-QB3 method. In the original CBS-QB3, CBS-Q energy calculations are combined with B3LYP/CBSB7-optimized geometries and frequencies. The five-step series of calculations starts with a geometry optimization at the B3LYP level, followed by a frequency calculation to obtain thermal corrections, zero-point vibrational energy, and entropic information. The next three calculations are single-point calculations at the CCSD(T), MP4SDQ, and MP2 levels. The CBS extrapolation then gives final energies. In the CBS-QB3//ωB97X-D method herein, the potential energy obtained from CBS-QB3 was corrected for the zero-point energy calculated at the ωB97X-D/6-311++G(d,p) level. The performance of the CBS-QB3//ωB97X-D method for various gas-species was assessed and validated in Matsugi and Shiina work[31)]. When investigating liquid reactions, solvent effects were included by applying the self-consistent reaction field (SCRF) option and polarizable continuum model (PCM) options[32)] within the program. Unfortunately, the dielectric constant of molten GN and other solvent parameters are not available; therefore, we used the value for water to determine the solvent effect when examining reactions in molten GN. Yamashita and Asai[33)] measured the ε of ammonium nitrate (AN), which is typical protic nitrate salt in analogy with GN. The dielectric constant for AN has been reported to be approximately 40 [-] at 383 K, and it is also reported that this value tends to increase along with temperature[33)]. Our previous study[34)] showed the total electron energies of the AN molecule as obtained using the ωB97X-D/6-311++G(d,p) method together with varying values of ε. Employing different dielectric constants had minimal impacts on the total energy at 0 K and the free-energy change of NH_4^+ + HNO_3 reaction, which is similar reaction to $CN_3H_6^+$ + HNO_3, at sufficiently high values of ε (> 30).

In the case of each reaction addressed in this paper, both the total energy change at 0 K (ΔE_0) and the Gibbs free energy (ΔG_{298}) between the TS and the reactants were considered. It should be noted that all chemical-reaction predictions take the free energy into account. However, to date, no methods that provide accurate free energy values for liquid-phase molecules have been established. The contribution of solvent effects obtained using the SCRF is normally added to the electronic energy using a standard quantum chemical approach. Other contributions to the enthalpy and entropy are evaluated by employing a formalism based on statistical mechanics, in conjunction with the ideal gas assumption, although this approach may lead to errors when computing the free energy values of liquid species. The effect of the nuclear motions of the solute species, which is not explicitly included in the SCRF method, also contributes to the thermodynamic properties of the system. Ishikawa and Nakai[35)] reported that mean absolute deviations for the Gibbs energies of the formation and combustion reactions of simple organic molecules obtained based on results from quantum chemistry calculation with PCM model were 49.6 and 26.7 kJ mol^{-1}, respectively.

3. Results and discussion

Details of these reaction pathways are discussed in the following sections, while all structures of reactants and products in this paper are provided in Figure 1.

3.1 Decomposition of guanidine

This work identified and investigated decomposition of guanidine (CN_3H_5) involving monomolecular reaction, bimolecular reaction, and cation-neutral bimolecular reaction. Their respective energy barriers and energy changes calculated at the CBS-QB3//ωB97X-D/6-311++G(d,p)/SCRF=(solvent = water) levels of theory, are listed in Table 1. First, the monomolecular reaction is shown below.

$$CN_3H_5 \rightarrow INT1 \quad (R1)$$
$$INT1 \rightarrow HNCNH + NH_3 \quad (R4)$$

CN_3H_5 isomerizes to INT1 via intramolecular hydrogen transfer and the INT1 promptly decompose to yield HNCNH and NH_3. The entire monomolecular reaction can be reduced to one equation: $CN_3H_5 \rightarrow HNCNH + NH_3$. This work has revealed that some species (M) aids the decomposition by assisting this intramolecular hydrogen transfer.

$$CN_3H_5 + M \rightarrow INT1 + NH_3 + M \quad \text{where M is } H_2O \text{ and } CN_3H_6^+ \quad (R2 \text{ and } R3)$$

Here, NH_4^+ and HNO_3 are more efficient catalysts (M) for CN_3H_5 decomposition due to a one-step conversion to HNCNH and NH_3 with a lower energy barrier.

$$CN_3H_5 + M \rightarrow HNCNH + NH_3 + M \quad \text{where M is } NH_4^+ \text{ and } HNO_3 \quad (R5 \text{ and } R6)$$

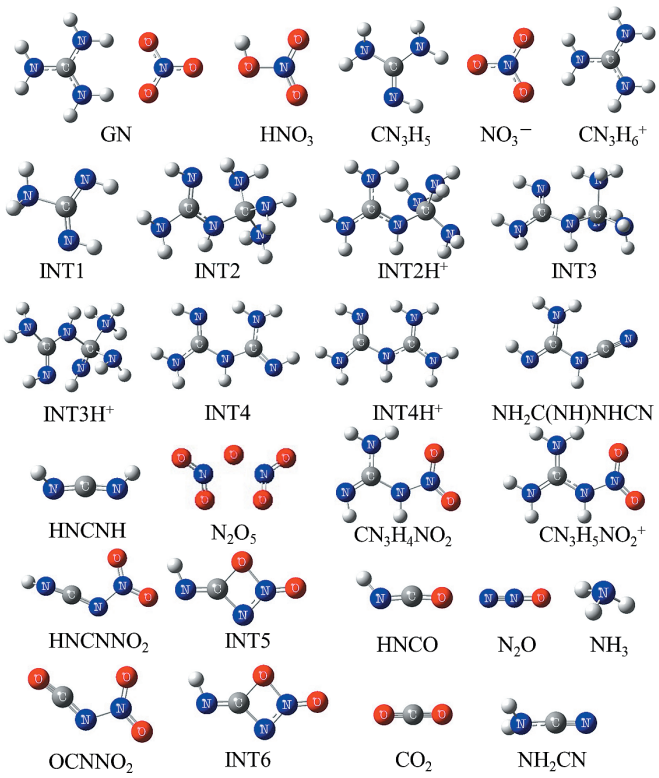

Figure 1 Chemical structures of reactants, products and intermediates in GN decomposition as optimized at the ωB97X-D/6-311++G(d,p)/SCFR = (solvent = water) level of theory.

Figure 2 shows the potential free-energy profiles for the reactions, including the optimized structures of the TSs. In the view of energy barrier, HNO_3 catalyzed monomolecular decomposition (R6) is the most plausible in these reactions. The associated free-energy barrier of this reaction is determined to be 108.9 kJ mol^{-1}.

Then, this work identified a bimolecular decomposition path, as shown below.

$$CN_3H_5 + CN_3H_5 \rightarrow INT2 \quad (R7)$$
$$INT2 \rightarrow INT3 \quad (R8)$$
$$INT3 \rightarrow INT4 + NH_3 \quad (R9)$$
$$INT4 \rightarrow NH_2C(NH)NHCN + NH_3 \quad (R10)$$
$$NH_2C(NH)NHCN \rightarrow HNCNH + NH_2CN \quad (R14)$$

Figure 3 shows the potential free-energy profiles for these reactions, including the optimized structures of the TSs. Two guanidine bonds to forms the dimer (INT2) as TS7. INT2 transforms to INT3 in manner of intramolecular proton transfer (TS8) and the INT3 decompose to yield INT3 and NH_3 (TS9). Some species (M) aids the decomposition by assisting this intramolecular hydrogen transfer (R11, R12, and R13 in Table 1). $NH_2C(NH)NHCN$ finally decompose to yield HNCNH and NH_2CN. The NH_2CN can isomerize to HNCNH. The entire bimolecular reaction can be reduced to one equation: $CN_3H_5 \rightarrow HNCNH + NH_3$. The associated free-energy barrier of this series reaction is determined to be 156.6 kJ mol^{-1} and the value is much higher than one of R6. Thus, the series of reaction can be negligible in possible the decomposition pathways of GN.

The last reactions, the cation-neutral bi-molecular reaction, are identified, as shown below.

$$CN_3H_5 + CN_3H_6^+ \rightarrow INT2H^+ \quad (R15)$$
$$INT2H^+ \rightarrow INT3H^+ \quad (R16)$$
$$INT3H^+ \rightarrow INT4H^+ + NH_3 \quad (R17)$$
$$INT4H^+ + CN_3H_5 \rightarrow INT4 + CN_3H_6^+ \quad (R18)$$

Kumbhakarna et al.[26] studied guanidinium azotetrazolate decomposition inculuding CN_3H_5 and $CN_3H_6^+$ and they reported similar mechanism. In their mechanism, $INT4H^+$ combined CN_3H_5 to yield NH_3 and a larger molecule, followed R17. Figure 4 shows the potential free-energy profiles for these reactions, including the optimized structures of the TSs. Guanidium cation ($CN_3H_6^+$) combines CN_3H_5 to forms the dimer cation ($INT2H^+$) as TS15. The dimer transforms to $INT3H^+$ in manner of intramolecular proton transfer (TS16) and the $INT3H^+$ decompose to yield $INT4H^+$ and NH_3 (TS17). Surrounding anions or bases might deprotonate $INT4H^+$ to form INT4. Following reaction is same to the neutral-neutral bimolecular mechanism. The entire cation-neutral bimolecular reaction can also be reduced to one equation: $CN_3H_5 \rightarrow HNCNH + NH_3$. The associated maximum energy barrier is determined to be 106.0 kJ mol^{-1} (R15) and the value is same or little less than one of R5. Although both R15 and R5 have similar free-energy barrier, the R15 is much large endothermic reaction. In addition to this, R 16 followed by R15 is also large endothermic reaction. Thus, we conclude that R15-R18 mechanism is not

Table 1 Reactions in the decomposition of guanidine with thermodynamic parameters calculated at the CBS-QB3//ωB97X-D/6-311++G(d,p)/SCRF = (solvent = water) levels of theory.

No.	Reaction	$\Delta E_0^{\ddagger}$ [1]	$\Delta_r E_0$ [2]	$\Delta G_{298}^{\ddagger}$ [1]	$\Delta_r G_{298}$ [2]
	unimolecular reaction				
R1	$CH_5N_3 \rightleftharpoons$ INT1	201.6	119.0	201.9	117.8
R2	$CH_5N_3 + H_2O \rightleftharpoons$ INT1 + H_2O	101.8	119.0	139.3	117.8
R3	$CH_5N_3 + CH_6N_3^+ \rightleftharpoons$ INT1 + $CH_6N_3^+$	90.1	119.0	135.7	117.8
R4	INT1 $\rightleftharpoons NH_3$ + HNCNH	45.4	−47.6	41.9	−85.9
R5	$CH_5N_3 + NH_4^+ \rightleftharpoons NH_3$ + HNCNH + NH_4^+	115.3	71.5	145.8	31.9
R6	$CH_5N_3 + HNO_3 \rightleftharpoons NH_3$ + HNCNH + HNO_3	68.8	71.5	108.9	31.9
	neutral-neutral bimolecular reaction				
R7	$CH_5N_3 + CH_5N_3 \rightleftharpoons$ INT2	104.8	12.5	156.6	66.2
R8	INT2 $\rightleftharpoons$ INT3	211.9	166.2	211.0	165.2
R9	INT3 $\rightleftharpoons$ INT4 + NH_3	0.4	−190.5	1.0	−235.7
R10	INT4 $\rightleftharpoons$ INT5 + NH_3	253.6	66.6	254.1	22.1
R11	INT4 + $NH_4^+ \rightleftharpoons NH_2C(NH)NHCN + NH_3 + NH_4^+$	101.3	66.6	132.5	22.1
R12	INT4 + $CH_6N_3^+ \rightleftharpoons NH_2C(NH)NHCN + NH_3 + CH_6N_3^+$	118.1	66.6	163.1	22.1
R13	INT4 + $HNO_3 \rightleftharpoons NH_2C(NH)NHCN + NH_3 + HNO_3$	72.0	66.6	110.8	22.1
R14	$NH_2C(NH)NHCN \rightleftharpoons$ HNCNH + NH_2CN	173.0	62.2	173.0	17.8
	ion-neutral bimolecular reaction				
R15	$CH_5N_3 + CH_6N_3^+ \rightleftharpoons INT2H^+$	54.6	5.8	106.0	59.3
R16	$INT2H^+ \rightleftharpoons INT3H^+$	36.4	40.4	37.9	41.6
R17	$INT3H^+ \rightleftharpoons INT4H^+ + NH_3$	21.0	−42.8	19.6	−89.0
R18	$INT4H^+ + CH_5N_3 \rightleftharpoons$ INT4 + $CH_6N_3^+$	–	−15.1	–	−16.3

[1] Energy barrier in the forward direction [kJ mol^{-1}] [2] Total energy change of reaction [kJ mol^{-1}]

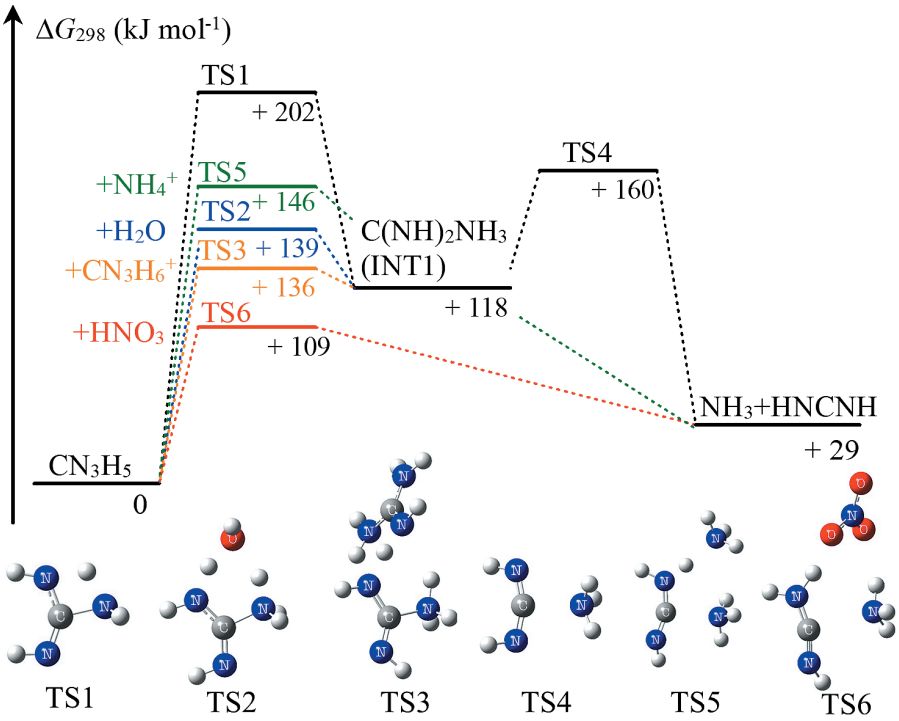

Figure 2 Potential free-energy profiles for the unimolecular decomposition of guanidine. The energy profiles were calculated at the CBS-QB3//ωB97X-D/6-311++G(d,p) SCFR = (solvent = water) level of theory.

thermodynamically preferable in the decomposition pathways of GN, although both of schemes are almost kinetically equal.

3.2 Guanidine + nitric acid

Onium-type nitrates including GN generally dissociate to HNO_3 (acid) and base compound (CN_3H_5 in case of GN) and the decomposition starts with HNO_3 attacking base compound. This work investigated three types of reactions between CN_3H_5 and HNO_3 analogous to ammonium nitrate decomposition[32]. Their respective energy barriers and energy changes calculated at the CBS

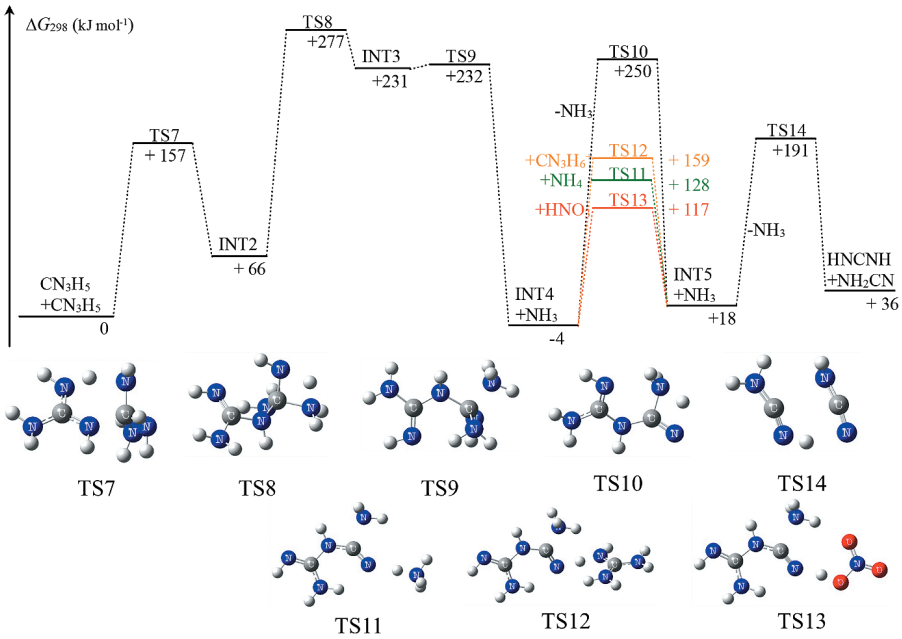

Figure 3 Potential free-energy profiles for the neutral-neuttral bimolecular decomposition of guanidine. The energy profiles were calculated at the CBS-QB3//ωB97X-D /6-311++G(d,p)/SCFR = (solvent = water) level of theory.

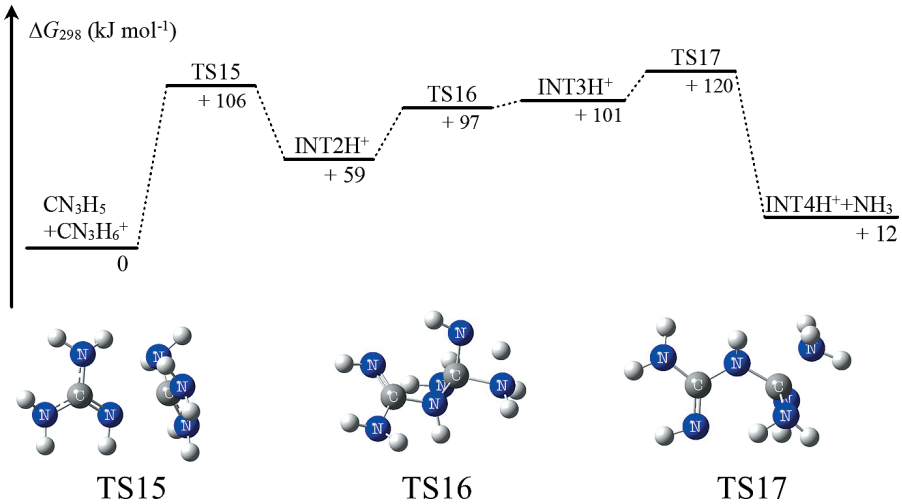

Figure 4 A potential free-energy profiles for the ion-neuttral bimolecular decomposition of guanidine. The energy profiles were calculated at the CBS-QB3//ωB97X-D /6-311++G(d,p)/SCFR = (solvent = water) level of theory.

-QB3//ωB97X-D/6-311++G(d,p)/SCRF=(solvent = water) levels of theory, are listed in Table 2. The first one is neutral-neutral bi-molecular reaction between HNO_3 and CN_3H_5.

$$CN_3H_5 + HNO_3 \rightarrow CN_3H_4NO_2 + H_2O \quad \text{(R19)}$$
$$CN_3H_4NO_2 \rightarrow \textit{trans}\text{-}NHNO_2H + HNCNH \quad \text{(R20)}$$

Figure 5 shows the potential free-energy profiles for the series of reactions, including the optimized structures of the TSs. In the mechanism that proceeds via TS19, cleavage of the N-OH bond in HNO_3 triggers its decomposition and the resulting OH· subtract H· from CN_3H_5 and NO_2· combines with CN_3H_4· to form nitroguanidine ($CN_3H_4NO_2$) and H_2O. The $CN_3H_4NO_2$ then decomposes to *trans*-$NHNO_2H$ and HNCNH through the cleavage of C-$NHNO_2$ bond and the H· transfer from NH_2 in NH_2CNH· to O- in $NHNO_2$· (TS20) as shown in Figure 6. The *trans*-$NHNO_2H$ decomposes to N_2O and H_2O ($NHNO_2H \rightarrow N_2O + H_2O$)[32]. The entire bimolecular reaction can be reduced to one equation: $CN_3H_5 + HNO_3 \rightarrow HNCNH + N_2O + 2H_2O$. The associated maximum energy barrier is determined to be 240.4 kJ mol^{-1} (R19). the value is much higher than those associated with other mechanisms, as discussed further on.

The second reaction is ion-neutral bi-molecular reactions

$$CN_3H_6^+ + HNO_3 \rightarrow CN_3H_5NO_2^+ + H_2O \quad \text{(R21)}$$
$$CN_3H_5NO_2^+ + NO_3^- \rightarrow CN_3H_4NO_2 + HNO_3 \quad \text{(R22)}$$

Figure 7 shows the potential free-energy profiles for the series of reactions, including the optimized structures of the TS21. This reaction starts with a proton transfer from $CN_3H_6^+$ to HNO_3, after which the protonated $H_2NO_3^+$ decomposes to H_2O and NO_2^+. The NO_2^+ then combines with CN_3H_5 to form $CN_3H_5NO_2^+$. The free-energy barrier was calculated to be 212.4 kJ mol^{-1}. The resulting $CN_3H_5NO_2^+$ is evidently deprotonated by NO_3^- (R22), which is

Table 2 Reactions in the interaction of CN_3H_5 and HNO_3 with thermodynamic parameters calculated at the CBS-QB3//ωB97X-D/6-311++G(d,p)/SCRF = (solvent = water) levels of theory.

No.	Reaction	$\Delta E_0^{\ddagger}$ [1]	$\Delta_r E_0$ [2]	$\Delta G_{298}^{\ddagger}$ [1]	$\Delta_r G_{298}$ [2]
R19	$CH_5N_3 + HNO_3 \rightleftharpoons CH_4N_3NO_2 + H_2O$	191.0	−51.5	240.4	−41.9
R20	$CH_4N_3NO_2 \rightleftharpoons$ *trans*-$HNNO_2H + HNCNH$	127.8	95.1	126.2	48.3
R21	$CH_6N_3^+ + HNO_3 \rightleftharpoons CH_5N_3NO_2^+ + H_2O$	168.7	2.6	212.4	8.5
R22	$CH_5N_3NO_2^+ + NO_3^- \rightleftharpoons CH_4N_3NO_2 + HNO_3$	–	35.1	–	34.8
R23	$HNO_3 + HNO_3 \rightleftharpoons N_2O_5 + H_2O$	89.8	40.1	129.5	46.1
R24	$CH_5N_3 + N_2O_5 \rightleftharpoons CH_4N_3NO_2 + HNO_3 + H_2O$ (TS16)	17.5	−91.6	67.6	−89.8
R25	$CH_6N_3^+ + N_2O_5 \rightleftharpoons CH_5N_3NO_2^+ + HNO_3 + H_2O$ (TS17)	158.6	−37.5	196.2	−39.4

[1] Energy barrier in the forward direction [kJ mol^{-1}] [2] Total energy change of reaction [kJ mol^{-1}]

plentiful in molten GN solutions, to give $CN_3H_4NO_2$. The $CN_3H_4NO_2$ decomposition process has already been showed above. The entire reaction can be also reduced to one equation: $CN_3H_5 + HNO_3 \rightarrow HNCNH + N_2O + 2H_2O$. Although the energy barrier values determined for this cation-neutral bimolecular reaction are lower than that for neutral-neutral bimolecular reaction, these values are still much higher than those associated with other mechanisms, as discussed further on.

The last reaction is HNO_3 self-decomposition path, as shown below.

$$HNO_3 + HNO_3 \rightarrow N_2O_5 + H_2O \quad \text{(R23)}$$

The same reaction was previously theoretically investigated[32]. The energy barrier and heat of reaction were determined to be 129.5 and 46.1 kJ mol^{-1}.

The produced N_2O_5 can attack neutral CN_3H_5 or cation $CN_3H_6^+$.

$$CN_3H_5 + N_2O_5 \rightarrow CN_3H_4NO_2 + HNO_3 \quad \text{(R24)}$$
$$CN_3H_6^+ + N_2O_5 \rightarrow CN_3H_5NO_2^+ + HNO_3 \quad \text{(R25)}$$

Figures 8 and 9 shows the potential energy profile for R24 and R25 with the optimized structures. The energy barrier for R24 was calculated as 67.6 kJ mol^{-1}. The neutral-neutral reaction of N_2O_5 and CN_3H_5 begins with the decomposition of N_2O_5 to $NO_2^{\cdot}$ and $NO_3^{\cdot}$, and the resulting $NO_2^{\cdot}$ immediately combines with NH_2 in CN_3H_5 to form $CN_3H_5NO_2^{\cdot}$ as TS24. The NO_3 removes H· from $CN_3H_5NO_2$ to yield $CN_3H_4NO_2$ and HNO_3. The $CN_3H_4NO_2$ decomposition process has already been discussed above. The entire reaction can be also reduced to one equation: $CN_3H_5 + HNO_3 \rightarrow HNCNH + N_2O + 2H_2O$. Because the energy barrier associated with R23 is higher than the values for R24, the rate determining step is R23. The cation-neutral reaction of $CN_3H_6^+$ and N_2O_5 starts with the decomposition of N_2O_5 to NO_2^+ and NO_3^-, which removes a proton from $CN_3H_6^+$ to give HNO_3 and CN_3H_5 as TS25. The dissociated NO_2^+ combines with CN_3H_5 to yield $CN_3H_5NO_2^+$. The decomposition of $CN_3H_5NO_2^+$ has been discussed above. The energy barrier of R25 was determined to be 196.2 kJ mol^{-1}. Because the energy barrier associated with R25 is much higher than the values for R24, R25 can be omitted from prefferable pathways.

Although all mechanism can be reduced to one equation: $CN_3H_5 + HNO_3 \rightarrow HNCNH + N_2O + 2H_2O$, self-decomposition mechanism of HNO_3 (ΔG = 129.5 kJ mol^{-1}) and followed $CN_3H_5 + N_2O_5$ (ΔG = 67.6 kJ mol^{-1}) reaction have the most plausible free-energy barrier in the interaction mechanism of CN_3H_5 and HNO_3 investigated in this study.

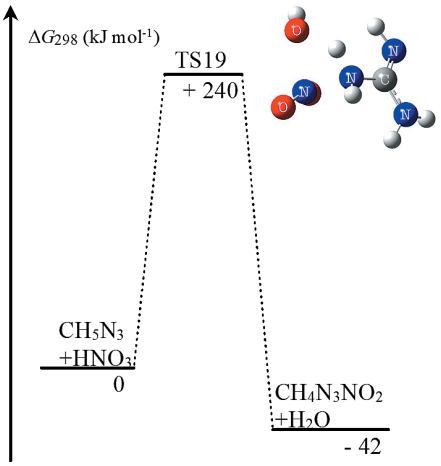

Figure 5 A potential free-energy profile for the CN_3H_5 + HNO_3 decompositions. The energy profiles were calculated at the CBS-QB3//ωB97X-D/6-311++G(d,p)/SCFR = (solvent = water) level of theory.

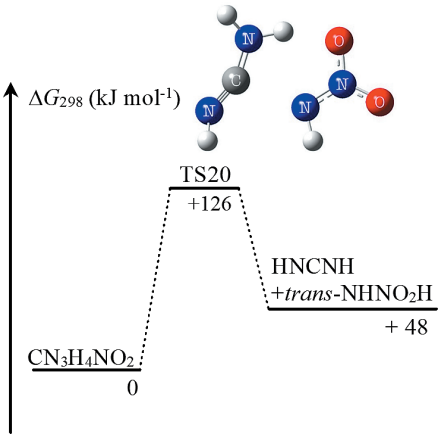

Figure 6 A potential free-energy profile for the decomposition of $CN_3H_4NO_2$. The energy profiles were calculated at the CBS-QB3//ωB97X-D/6-311++G(d,p)/SCFR = (solvent = water) level of theory.

3.3 Decomposition of intermediates

As discussed above, HNCNH ($\rightleftharpoons NH_2CN$) is one of the major products from CN_3H_5 decomposition and interaction of CN_3H_5 and HNO_3. This work investigated the reactions

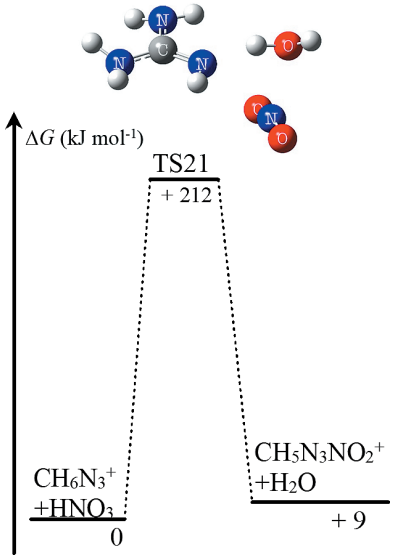

Figure 7 A potential free-energy profile for the $CN_3H_6^+$ + HNO_3 decomposition. The energy profiles were calculated at the CBS-QB3//ωB97X-D/6-311++G(d, p)/SCFR = (solvent = water) level of theory.

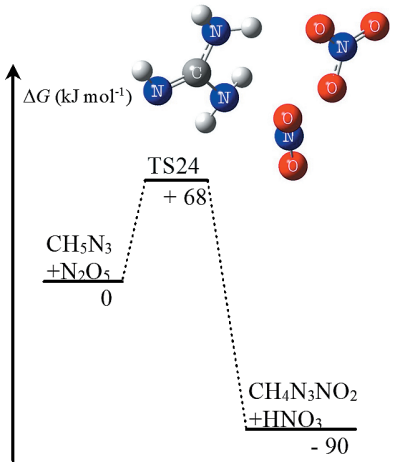

Figure 8 A potential free-energy profile for the CN_3H_5 + N_2O_5 reaction. The energy profiles were calculated at the CBS-QB3//ωB97X-D/6-311++G(d, p)/SCFR = (solvent = water) level of theory.

associated with HNCNH. Their respective energy barriers and energy changes calculated at the CBS-QB3//ωB97X-D/6-311++G (d,p)/SCFR = (solvent = water) levels of theory, are listed in Table 3.

$$HNCNH + N_2O_5 \rightarrow HNCNNO_2 + HNO_3 \quad (R26)$$
$$HNCNNO_2 \rightarrow INT5 \quad (R27)$$
$$INT5 \rightarrow HNCO + N_2O \quad (R28)$$

$$HNCO + N_2O_5 \rightarrow OCNNO_2 + HNO_3 \quad (R29)$$
$$OCNNO_2 \rightarrow INT6 \quad (R30)$$
$$INT6 \rightarrow CO_2 + N_2O \quad (R31)$$

Figures 10 and 11 show the potential free-energy profiles for the series of reactions, including the optimized structures of the TSs. Previous study reported N_2O, HNCO and CO_2 is the major evolved gases[36]. This study also reveals the evolving pathways of the gases.

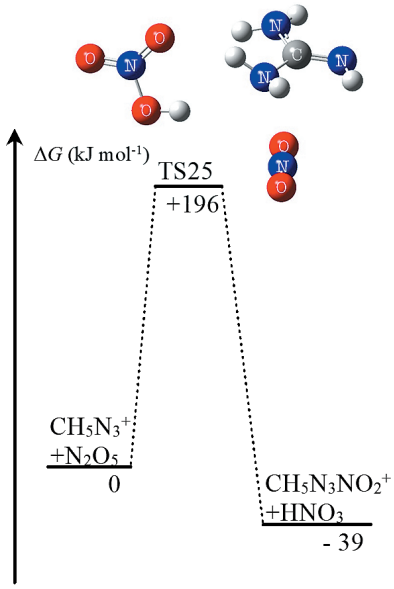

Figure 9 A potential free-energy profile for the $CN_3H_6^+$ + N_2O_5 reaction. The energy profiles were calculated at the CBS-QB3//ωB97X-D/6-311++G(d,p)/SCFR = (solvent = water) level of theory.

3.4 Initial reaction pathway

Various sets of GN reactions were investigated in this study. We divided the GN reactions into two groups, decomposition of CN_3H_5 and reaction of CN_3H_5 and HNO_3. In decomposition of CN_3H_5 mechanism, HNO_3 catalyzed decomposition is the most plausible, as following

$$CH_5N_3 + HNO_3 \rightarrow HNCNH + NH_3 + HNO_3$$

In reaction of CN_3H_5 and HNO_3, self-decomposition of HNO_3 trigger the reaction. The schemes below summarize the sets of reactions investigated in this study.

$$GN \rightarrow HNO_3 + CH_5N_3$$
$$HNO_3 + HNO_3 \rightarrow N_2O_5 + H_2O$$
$$CH_5N_3 + N_2O_5 \rightarrow CH_4N_3NO_2 + HNO_3$$
$$CH_4N_3NO_2 \rightarrow \textit{trans}\text{-}NHNO_2H + HNCNH$$
$$\textit{trans}\text{-}NHNO_2H \rightarrow N_2O + H_2O$$
$$\text{(overall) } GN \rightarrow HNCNH + N_2O + 2H_2O$$

In the initial decomposition pathways of GN, these two reactions occur in parallel. HNCNH produced from both initial reaction is oxidized by N_2O_5 to form N_2O and HNCO, which is finally decompose to CO_2. Miyake et al.[36] measured the evolved gas from decomposition of GN using with TG-DTA-MS and TG-DTA-IR, and they reported that the evolved gas consisted of NH_3, H_2O, N_2 (minor), HNCO, CO_2, and N_2O. The mechanism developed from this study can provide good explanation to experimental gas-evolving behavior. The new mechanism, however, has not included N_2 gas generating. N_2 gas might be evolved from radical reaction which is triggered by the homolytic cleavage of HNO_3. Thus, further study has still been needed to fully clear the mechanism of thermal decomposition of GN.

4. Conclusions

The thermal decomposition reactions of guanidine nitrate (GN) in the liquid phase were investigated based

Table 3 Reactions in the decomposition of intermediates with thermodynamic parameters calculated at the CBS-QB3//ωB97X-D/6-311++G(d,p)/SCRF = (solvent = water) levels of theory.

No.	Reaction	$\Delta E_0^{\ddagger}$ [1]	$\Delta_r E_0$ [2]	$\Delta G_{298}^{\ddagger}$ [1]	$\Delta_r G_{298}$ [2]
R26	HNCNH+ N_2O_5 ⇌ $HNCNNO_2$ + HNO_3 (TS17)	31.0	−65.8	67.8	−68.0
R27	$HNCNNO_2$ ⇌ INT5 (TS3)	69.5	34.8	72.8	38.7
R28	INT5 ⇌ HNCO + N_2O (TS3)	34.3	−306.2	33.2	−349.3
R29	HNCO+ N_2O_5 ⇌ $OCNNO_2$ + HNO_3 (TS17)	45.2	−31.7	85.3	−33.1
R30	$OCNNO_2$ ⇌ INT6 (TS3)	53.2	33.8	56.9	37.5
R31	INT6 ⇌ CO_2 + N_2O (TS3)	10.7	−345.2	10.1	−380.9

[1] Energy barrier in the forward direction [kJ mol^{-1}] [2] Total energy change of reaction [kJ mol^{-1}]

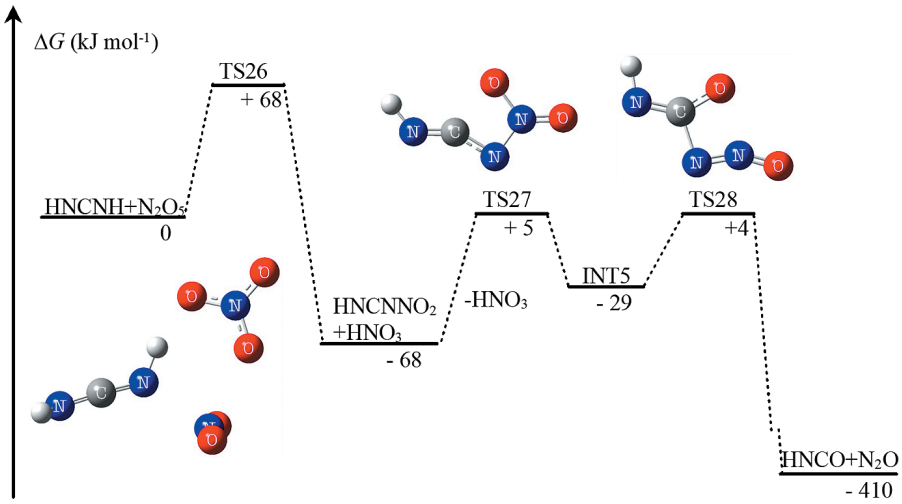

Figure10 A potential free-energy profile for the HNCNH + N_2O_5 and followed reaction. The energy profiles were calculated at the CBS-QB3//ωB97X-D/6-311++G(d,p)/SCFR = (solvent = water) level of theory.

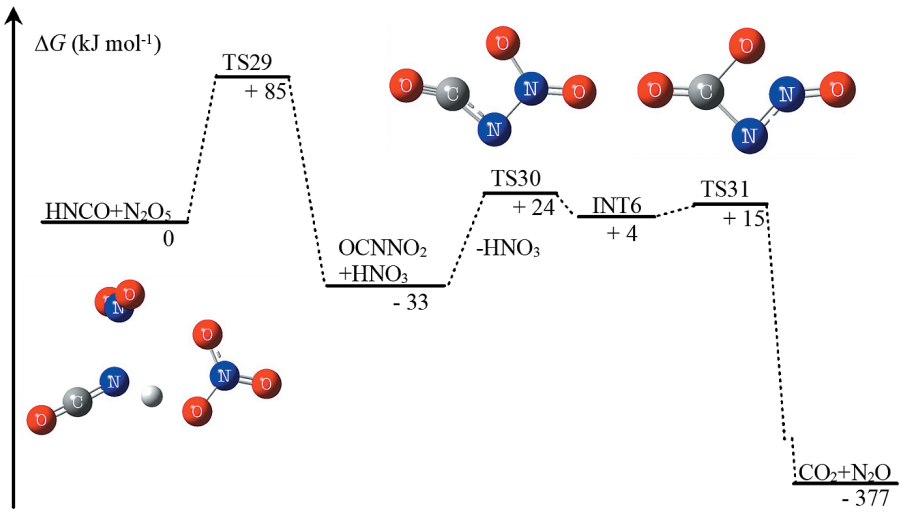

Figure11 A potential free-energy profiles for the HNCO + N_2O_5 and followed reactions. The energy profiles were calculated at the CBS-QB3//ωB97X-D/6-311++G(d,p)/SCFR = (solvent = water) level of theory.

on DFT calculations. These calculations were performed at the ωB97X-D/6-311++G (d,p) and CBS-QB3//ωB97X-D/6-311++G (d,p) levels of theory.

The reaction pathways of decomposition of CN_3H_5 were investigated. Mechanisms for the neutral monomolecular decomposition (CN_3H_5 → NH_3 + HNCNH), neutral-neutral bimolecular decomposition (CN_3H_5 + CN_3H_5), and ion-neutral bimolecular reaction (CN_3H_5 + $CN_3H_6^+$) were developed. In the mechanisms, HNO_3 catalyzed monomolecular decomposition have the most plausible energy barrier.

The CN_3H_5/HNO_3 reaction pathways were investigated. We developed four mechanisms and each of these schemes provided the same global reaction: CN_3H_5 + HNO_3 → HNCNH + N_2O + $2H_2O$. These schemes can be divided according to combinations of oxidizers (HNO_3 or N_2O_5) and reductants (CN_3H_5 or $CN_3H_6^+$). Based on the energy barrier calculations, the N_2O_5/CN_3H_5 scheme is the

most plausible. HNCNH from initial decomposition oxidized by N_2O_5 to form N_2O, HNCO, CO_2.

This study has revealed the initial decomposition pathways of GN. The mechanism can provide good explanation to experimental gas-evolving behavior. To model the detailed kinetics of liquid decomposition of GN, radical reaction mechanism is needed in addition to the initial decomposition. In the future work, the mechanisms will be developed and the detailed kinetic model will be established.

Acknowledgement

This research was supported by the Foundation for the Promotion of Industrial Explosives Technology 2017.

References

1) Y. N. Matyushin, T. S. kon'kova, K. V. Titova, V. Ya. Rosolovskii, and Y. A. Lebedev, Bulletin of the Academy of Sciences of the USSR, Division of Chemical Science, 34, 716−719 (1985).
2) J. W. Schoppelrei, M. L. Kieke, X. Wang, M. T. Klein, and T. B. Brill, J. Phys. Chem., 100, 14343−14351 (1996).
3) M. R. Udupa, Thermochemica Acta., 53, 383−385 (1982).
4) Y. I. Rubtsov, A. I. Kazakov, D. B. Lempert, and G. B. Manelis, Russ. J. Appl. Chem., 77, 1083−1091 (2004).
5) R. S. Damse, J. Hazardous Materials, 172, 1383−1387 (2009).
6) J. C. Oxley, J. L. Smith, E. Rogers, W. Naik, and J. Moran, J. Energ. Mater., 27, 17−39 (2008).
7) M. Nakashima, T. Itaura, H. Matusnaga, E. Higashi, S. Takagi, and K. Katoh, J. Therm. Anal. Calorim. 135, 95−100 (2018).
8) S. Yoshino and A. Miyake, J. Therm. Anal. Calorim., 102, 513−516 (2010).
9) X. Mei, Y. Cheng, Y. Li, X. Zhu, S. Yan, and X. Li, J. Therm. Anal. Calorim., 114, 131−135 (2013).
10) A. Ulas, G. A. Risha, and K. K. Kuo, Fuel, 85, 1979−1986 (2006).
11) Y. Izato and A. Miyake, Proc. Spring Conference of Japan Explosive Society, 120−123, Japan Explosive Society, Tokyo (2017). (in Japanese).
12) V. P. Sinditskii, V. Y. Egorshev, V. V. Serushkin, and S. A. Filatov, Combust Explos Shock Waves, 48, 81−99 (2012).
13) Y. Izato, S. Date, and A. Miyake, Propellants, Explos. Pyrotech., 38, 129−135 (2013).
14) P. Thakre, Y. Duan, and V. Yang, Combust. Flame, 161, 347−362 (2014).
15) J. Park and M. C. Lin, J. Phys. Chem. A, 113, 13556−13561 (2009).
16) J. Park, D. Chacraborty, and M. C. Lin, Symp. (Int.) on Combust. 27, 2351−2357 (1998).
17) Y. Daimon, H. Terashima, and M. Koshi, J. Propul. Power, 30, 707−716 (2014).
18) N. E. Ermolin, Combust. Explos. Shock Waves, 40, 92−109 (2004).
19) N. E. Ermolin, Combust. Explos. Shock Waves, 43, 549−561 (2007).
20) Y. Izato, M. Koshi, and A. Miyake, Sci. Tech. Energetic Materials, 78, 12−18 (2017).
21) Y. Izato and A. Miyake, Sci. Tech. Energetic Materials, 78, 143−149 (2017).
22) N. E. Ermolin, O. P. Korobeinichev, A. G. Tereshchenko, and V. M. Fomin, Combust. Explos. Shock Waves, 18, 180−189 (1982).
23) S. Raman, R. W. Ashcraft, M. Vial, and M. L. Klasky, J. Phys. Chem. A, 109, 8526−8536 (2005).
24) R. W. Ashcraft, S. Raman, and W. H. Green, J. Phys. Chem. B, 111, 11968−11983 (2007).
25) R. W. Ashcraft, S. Raman, and W. H. Green, J. Phys. Chem. A, 112, 7577−7593 (2008).
26) N. R. Kumbhakarna, K. J. Shah, A. Chowdhury, and S. T. Thynell, Thermochim Acta, 590, 51−65 (2014).
27) N. Kumbhakarna and S. T. Thynell, Thermochim Acta, 582, 25−34 (2014).
28) J. D. Chai and M. Head-Gordon, Phys. Chem. Chem. Phys., 10, 6615−6620 (2008).
29) M. J. Frisch, G. W. Trucks, H. B. Schlegel, G. E. Scuseria, M. A. Robb, J. R. Cheeseman, G. Scalmani, V. Barone, B. Mennucci, G. A. Petersson, H. Nakatsuji, M. Caricato, X. Li, H. P. Hratchian, A. F. Izmaylov, J. Bloino, G. Zheng, J. L. Sonnenberg, M. Hada, M. Ehara, K. Toyota, R. Fukuda, J. Hasegawa, M. Ishida, T. Nakajima, Y. Honda, O. Kitao, H. Nakai, T. Vreven, J. A. Montgomery, J. E. Peralta, F. Ogliaro, M. Bearpark, J. J. Heyd, E. Brothers, K. N. Kudin, V. N. Staroverov, T. Keith, R. Kobayashi, J. Normand, K. Raghavachari, A. Rendell, J. C. Burant, S. S. Iyengar, J. Tomasi, M. Cossi, N. Rega, J. M. Millam, M. Klene, J. E. Knox, J. B. Cross, V. Bakken, C. Adamo, J. Jaramillo, R. Gomperts, R. E. Stratmann, O. Yazyev, A. J. Austin, R. Cammi, C. Pomelli, J. W. Ochterski, R. L. Martin, K. Morokuma, V. G. Zakrzewski, G. A. Voth, P. Salvador, J. J. Dannenberg, S. Dapprich, A. D. Daniels, O. Farkas, J. B. Foresman, J. V. Ortiz, J. Cioslowski, and D. J. Fox, Gaussian 09, Revision D.01, Gaussian, Inc., Wallingford CT (2010).
30) J. A. Montgomery, M. J. Frisch, J. W. Ochterski, and G. A. Petersson, J. Chem. Phys., 110, 2822−2827 (1999).
31) A. Matsugi and H. Shiina, Bull. Chem. Soc. Jpn., 87, 890−901 (2014).
32) J. Tomasi, B. Mennucci, and E. Cancès, J. Mol. Struct., 464, 211−226 (1999).
33) A. Yamashita and K. Asai, Phys. Soc. Japan, 18, 1247−1253 (1963).
34) Y. Izato, M. Koshi, and A. Miyake, Int. J. Chem. Kinet., 49, 83−99 (2017).
35) A. Ishikawa and H. Nakai, Chem. Phys. Lett., 624, 6−11 (2015).
36) A. Miyake, Y. Shimada, S. Yoshino, and A. Kimura, Sci. Tech. Energetic Materials, 74, 23−28 (2013).